The effect of type-B carbonate content on the elasticity of fluorapatite

The effect of type-B carbonate content on the elasticity of fluorapatite

Fernando Cámara, [1,2]

Nadia Curetti. [2,3] Please add ORCID ID: Nadia Curetti
https://orcid.org/0000-0002-6300-7133

Piera Benna, [2✉,3]

Phone 00-39-011-6705120
Email piera.benna@unito.it

Yassir A. Abdu. [4] Please add ORCD ID: Yassir A. Abdu
https://orcid.org/0000-0003-4432-6486

Frank C. Hawthorne, [5]

Cristiano Ferraris, [6]

[1] Dipartimento di Scienze della Terra “Ardito Desio”, Via Mangiagalli 34, 20133 Milano, Italy

[2] CrisDi Interdepartmental Center for Crystallography, Via P. Giuria 5, 10125 Torino, Italy

[3] Dipartimento di Scienze della Terra, Via Valperga Caluso 35, 10125 Torino, Italy

[4] Department of Applied Physics and Astronomy, University of Sharjah, P.O. Box 27272, Sharjah, UAE

[5] Department of Geological Sciences, University of Manitoba, 125 Dysart Road, Winnipeg, MB, R3T 2N2 Canada

[6] Institute of Mineralogy, Physics of Materials and Cosmochemistry UMR 7590, National History Museum of Natural Sciences, CP 52, 61 Rue Buffon, 75005 Paris, France

Received: 2 December 2017 / Accepted: 14 March 2018

Abstract

The mechanical behavior of carbonate-bearing fluorapatite (CFAP) (with up to 5.5 wt% CO_3) was investigated at high pressure up to 7 GPa. The incorporation of carbonate in CFAP samples was investigated by FTIR spectroscopy. The chemical formulae and cell parameters are $Ca_{4.90}Fe_{0.04}(PO_4)_{2.87}(CO_3)_{0.13}F_{1.23}$ and $a = 9.3527(1)$, $c = 6.8752(1)$ Å, $V = 520.83(1)$ Å^3 for the FOW CFAP (Fowey Consols area, UK), and $Ca_{4.97}Sr_{0.03}(PO_4)_{2.55}(CO_3)_{0.45}F_{1.42}$ and $a = 9.3330(1)$, $c = 6.8984(1)$ Å, $V = 520.38(1)$ Å^3 for the FRA CFAP (Framont region, France). Preliminary characterization at ambient conditions was done by single-crystal X-ray diffraction study. The structure refinements, in space group $P6_3/m$, confirm a type-B substitution of the phosphate $(PO_4)^{3-}$ group by the carbonate ion $(CO_3)^{2-}$. The site occupancies for the C atom are 0.04 for FOW and 0.11 for FRA CFAP, in quite good agreement with the 1.6 and 5.5 wt% CO_3 amount obtained by analytical methods. Single-crystal high-pressure XRD study on the two type-B CFAP samples was performed. The FOW and FRA crystals were mounted concurrently in a ETH-type DAC and cell parameters were determined at 26 different pressures up to 6.86 GPa at room *T*. The variation with pressure of the unit-cell parameters and volume shows no discontinuity that could be related to any possible phase transition in the *P* range investigated. The linear compressibility coefficients are $\beta_a = 3.63 \times 10^{-3}$ GPa^{-1} and $\beta_c = 2.47 \times 10^{-3}$ GPa^{-1} for FOW, and $\beta_a = 3.67 \times 10^{-3}$ GPa^{-1} and $\beta_c = 2.65 \times 10^{-3}$ GPa^{-1} for FRA, giving an axial anisotropy of β_a:β_c = 1.47:1 and 1.38:1, respectively. The *P*-*V* data were fitted by a second-order Birch–Murnaghan EoS and the resulting BM2-EoS coefficients are $V_0 = 519.81(7)$ Å^3, $K_{T0} = 92.1(3)$ GPa for FOW, and $V_0 = 518.95(9)$ Å^3, $K_{T0} = 89.1(4)$ GPa for FRA CFAP. The results obtained indicate that a 5.5 wt% CO_3 content (type-B) reduces the isothermal bulk modulus by about 9%.

Keywords

Carbonate-rich fluorapatite
FTIR spectra
HP SC-XRD
Crystal structure
Bulk modulus
EoS

Electronic supplementary material

The online version of this article (https://doi.org/10.1007/s00269-018-0962-1) contains supplementary material, which is available to authorized users.

Introduction

Apatite is an important mineral occurring in igneous, metamorphic and hydrothermal rocks and the knowledge of its mineral physics helps to assess the geological implications of its stability field. Understanding its stability at the Earth's interior is essential to grasp its role as a possible repository of phosphorous at mantle depths. Beside its potential application to mantle mineralogy, knowledge of the apatite Equation of State (EoS) is also relevant to metamorphic petrologic applications such as interpreting pressure–temperature–time paths (Brunet et al. 1999; Ashley et al. 2017). Apatite has many geological uses, including dating techniques and studies of the variation of rare-earth elements in rocks, and is also widely used in material science (Hughes 2015 and references therein). Rock phosphates (microcrystalline apatites), mostly of biological origin, are the starting material for the manufacture of phosphate fertilizer and a source of phosphorus for the chemical industry (Elliott et al. 2002; Rakovan and Pasteris 2015). In the biomedical field, its mechanical properties play a major role in its technological applications, as apatite is the main constituent of dental enamel and human bone (Elliott 1994, 2002; Pasteris 2016).

The apatite group has three calcium phosphate mineral species, fluorapatite (FAP), chlorapatite (CAP), and hydroxylapatite (HAP) with the general formula ~~of~~ Ca_5-$(PO_4)_3$-(F,Cl,OH) (Pasero et al. 2010). Recent attention has focused on a more complete understanding of the apatite atomic arrangement and its properties, both in inorganic and biogenic apatite, and knowledge of the details of its atomic arrangement is increasing (Hughes et al. 1989, 1990, 2014; Hughes and Rakovan 2002, 2015; McCubbin et al. 2008; Hughes 2015). It is well-established that the incorporation of carbonate into the apatite structure has a destabilizing effect, resulting in increased solubility (LeGeros 1991). Whereas the structural details of FAP, CAP, and HAP are generally well-established, those of "carbonated" apatite are not yet very clear (Liu et al. 2011; Yi et al. 2013). Due to the importance of carbonate-bearing HAP in biomineralization (Elliott 2002), the incorporation of carbonate into apatite and its resulting physical–chemical changes have been investigated extensively and yet are still not well understood (McClellan 1980; Perdikatsis 1991; Elliott 1994; Regnier et al. 1994; Nathan 1996; Wilson et al. 1999, 2004; Comodi and Liu 2000; Leventouri et al. 2000; Ivanova et al. 2001; Elliott et al. 2002; Pan and Fleet 2002; Fleet and Liu 2004, 2007, 2008a, b; Yi et al. 2013). Incorporation of carbonate into the apatite structure can occur by substitution for both channel anion (type-A) and phosphate ion (type-B), as first suggested by McConnell (1938). Several authors (LeGeros 1965; McClellan and Lehr 1969; McClellan and Van Kauwenbergh

1990) have shown a correlation between increased carbonate and decreased phosphate, with different effects on the unit-cell parameters (Knudsen and Gunter 2002). The response of the unit-cell parameters of apatite to accommodation of the carbonate ion is complicated (Elliott 2002; Fleet et al. 2004; Liu et al. 2011). Substitution of hydroxyl by type-A carbonate in the channels results in a progressive increase in *a* values and a decreasing trend for *c* values, whereas substitution of phosphate by type-B carbonate gives origin to inverse trends where *a* decreases and *c* increases. However, many of the type-B carbonate apatites have somewhat increased *a* dimensions due mainly to the vacancies in oxygen sites coordinating tetrahedra and the possible presence of Ca substituted by H_2O groups (Ivanova et al. 2001).

With regard to the elastic behavior of apatites, several compression experiments are done (Brunet et al. 1999; Comodi et al. 2001; Matsukage et al. 2004; Schouwink et al. 2010; Liu et al. 2011) ~~in Table 1~~ to investigate the compressibility of synthetic and natural apatite. Literature results are listed in Table 1 to compare the bulk modulus and the volume variations between the previous studies for apatite species and our results for carbonate-bearing fluorapatite (CFAP). Allan et al. (1996) and Brunet et al. (1999) studied the compressibility of three synthetic crystals of FAP, HAP, and CAP up to maximum pressures of 18, 20 and 52 GPa, respectively, at ambient temperature, by high-pressure synchrotron X-ray powder diffraction. Regardless of the large *P*-range, only the unit-cell volumes measured to about 10 GPa were used to derive their EoS, because higher-pressure data were affected by non-hydrostatic effects. A second-order Birch–Murnaghan EoS was fitted to the data giving values of $K_0 = 97.9$, 97.5, and 93.1 GPa for FAP, HAP, and CAP, respectively (Table 1). Because the three bulk moduli are identical within one estimated standard deviation, the halogen content of apatite was considered to not have a significant effect on volume compressibility, whereas the compressibility of *a* and *c* parameters seems more sensitive to halogen composition. Consistently, for each species, the *a*-axis is more compressible than the *c*-axis.

Table Note. In Tables 1,3,4,5,6, the (esd) values are separated by means of a space by their numbe
values are generally attacked, is this a new format of the magazine?
I mean: 522.4 (4) instead of 522.4(4)
Since you have separated them all in all the tables, you can also leave them like this, so as not to mak
you as you like, thank you **1**

Compression data for apatite in the *P* range: $0.0001 - P_{max}$

Reference	Composition	Diffraction techniques	P_{max} (GPa)	EoS	V_0 (Å^3)	K_T (G

Reference	Composition	Diffraction techniques	*P* (GPa)	EoS	*V* (Å)	*K* (G
Brunet et al. (1999)	FAP (synthetic)	Powder	10	BM2	522.4 (4)	97 (1.
Brunet et al. (1999)	HAP (synthetic)	Powder	10	BM2	526.9 (5)	97 (1.
Brunet et al. (1999)	CAP (synthetic)	Powder	10	BM2	539.3(1.4)	93 (4.
Comodi et al. (2001)	FAP (synthetic)	Single-crystal	6.9	BM2	–	97 (1.
				BM3	*524.21 (8)*	*93*
Matsukage et al. (2004)	$FAP_{94}CAP_6$	Powder	7.1	BM2	524.2 (2)	91 (1.
				BM3	524.2 (3)	*91 (3.*
Schouwink et al. (2010)	$FAP_{95}CAP_5$	Single-crystal	9.2	*BM3*	*525.89 (4)*	*88 (7)*
Liu et al. (2011)	CHAP (5 wt% CO_3) (synthetic)	Powder	10	BM2 *BM3* please split the words BM2*BM3* and wrap: BM2 *BM3*	529.16 (8)	89 (5)
					529.17 (9)	*89*
Liu et al. (2011)	CHAP (11 wt% CO_3) (synthetic)	Powder	10	BM2	527.1 (4)	84
				BM3	*527.5 (2)*	*73*
FOW (this study)	CFAP (1.6 wt% CO_3)	Single-crystal	6.9	BM2	519.81 (7)	92 (3)
FRA (this study)	CFAP (5.5 wt% CO_3)	Single-crystal	6.9	BM2	518.95 (9)	89 (4)

The parameters of the Birch–Murnaghan Equation of State (BM EoS) are: V_0 = zero-pres volume, K_{T0} isothermal bulk modulus, *K'* first pressure derivative of K_{T0} (esd in parenth *BM3* values are in italic

FAP fluorapatite, *HAP* hydroxylapatite, *CAP* chlorapatite, *CHAP* carbonate-bearing hydr *CFAP* carbonate-bearing fluorapatite

Comodi et al. (2001), using single-crystal XRD, determined the compressibility up to about 7 GPa of a synthetic fluorapatite with $a = 9.375(2)$, $c = 6.887(1)$ Å,

and $V = 524.23(5)$ Å^3 cell parameters. The compressibility along *a* was greater compared to the one measured along *c*. Unit-cell parameters showed a linear variation with *P* and their calculated linear compressibility coefficients give β_a:β_c = 1.38:1. Volume compressibility data fitted with BM3 EoS gave a bulk modulus of $K_0 = 93$ (Table 1), whereas data fitted with BM2 EoS gave a bulk modulus of $K_0 = 97.8$ GPa, in good accord with the value obtained by Brunet et al. (1999) in their fluorapatite, although the latter contained 0.025 apfu hydroxyl.

A fluorapatite of composition $FAP_{94}CAP_6$ was studied by Matsukage et al. (2004) by in-situ synchrotron X-ray powder diffraction up to 7.12 GPa at ambient temperature. Both unit-cell parameters and volume decrease systematically with increasing pressure ~~up to 7.12 GPa~~; a larger compression along *a* compared to the one along *c*, as previously observed in synthetic fluorapatite by Comodi et al. (2001), was observed. The BM3 EoS fitted to the volume–pressure data gave the isothermal bulk modulus $K_T = 91.5(3.8)$ GPa, and the error became smaller with K' fixed at 4 (BM2) (Table 1). The bulk modulus of Matsukage et al. (2004) for fluorapatite is about 6% lower compared to the values of Brunet et al. (1999) and Comodi et al. (2001). The unit-cell axial moduli were fitted by a BM2 EoS and gave $Ka_T = 80(1)$ and $Kc_T = 126(1)$ GPa for *a* and *c* axis, respectively, confirming that fluorapatite is elastically anisotropic. The anisotropy of the axial moduli was estimated to be about 58%.

Schouwink et al. (2010), studying ion tracks in apatite, performed high-pressure single-crystal XRD up to 10 GPa on irradiated and non-irradiated crystals of fluorapatite ($FAP_{95}CAP_5$), coming from Durango (Mexico). The values of bulk modulus are about 3–5% lower than the results reported by Matsukage et al. (2004) and Comodi et al. (2001) (Table 1). Regarding the axial compressibilities, the Authors confirm the previously determined elastic anisotropy with the *c*-axis being less compressible relative to the *a*-axis.

More recently, Liu et al. (2011) investigated the mechanical behavior of "carbonated" hydroxylapatite (CHAP) and studied the effect of carbonate ion on the compressibility of HAP. The incorporation of the carbonate oxy-anion (for both types A-B) into the structure of HAP results in the formation of vacancies, oxygen-loss and disorder, with consequent changes in the physical–chemical properties. Liu et al. (2011) results were obtained using a diamond-anvil cell and synchrotron X-ray powder diffraction up to 10 GPa on two synthetic CHAP samples with up to 11 wt% CO_3. The results of their BM3 EoS data-fitting, reported in Table 1, suggest that carbonate content significantly reduces the isothermal bulk modulus of CHAP (up to about 15%).

To clarify the influence on the elastic properties of the incorporation of carbonate into the structure of FAP, we have examined two type-B carbonate-bearing fluorapatites (CFAP) by H*P* single-crystal X-ray diffraction. The purpose of our study is to determine the Equation of State (Eos) and to understand the compressional properties of type-B CFAP.

Experimental methods

The two samples of carbonate-bearing fluorapatite (CFAP) are from the National History Museum of Natural Science of Paris (France). One is labeled "francolite" MNHN-63.116 (hereafter FOW), and comes from Fowey Consols area, St Austell District, Cornwall, England, UK (one of the deepest, richest and most important of the Cornish copper mines), and the other is labeled "francolite" MNHN-96.1356 (hereafter FRA) from the Framont-Grandfontaine region in Alsace, France (an ancient iron-mining area). "Francolite" is a carbonate-rich variety of fluorapatite, characterized by an excess amount of F, with carbonate groups $(CO_3)^{2-}$ partly substituting the phosphate $(PO_4)^{3-}$ ones. The name "francolite" comes from Wheal Franco (Tavistock District, Devon, England, UK) (Henry 1850; Sandell et al. 1939) and was used to identify apatite containing at least 1% fluorine and appreciable CO_3. The name "francolite" was afterwards discredited by IMA and replaced with "carbonate-rich" or "carbonate-bearing" fluorapatite (Pasero et al. 2010).

The fluorapatite samples were investigated by FTIR spectroscopy using a Bruker Hyperion 2000 IR microscope equipped with a liquid-nitrogen-cooled MCT detector. Spectra over the range 4000–650 cm^{-1} were obtained by averaging 100 scans with a resolution of 4 cm^{-1}. Base-line correction was done using the OPUS spectroscopic software (Bruker Optic GmbH). The spectra were collected on thin films having a similar thickness; to compare the IR intensity (absorbance) of the carbonate bands (proportional to concentration) for the two samples, the sizes of the selected crystal fragments used to obtain the films (via a diamond press) were very similar.

The chemical compositions of the crystals were obtained using a Cameca SX-100 electron microprobe operating in wavelength-dispersive mode with an accelerating voltage of 15 kV, a specimen current of 20 nA, and a beam diameter of 10 μm. The following standards were used: Si: diopside; F, Ca and P: apatite; Sr: $SrTiO_3$; Fe: fayalite. The elements Si, Na, La, Ce, Pr, Nd, Sm, Y, Mg, Cl and S were sought but were below detection limits. The data were reduced and corrected by the PAP method of Pouchou and Pichoir (1985). The CO_2 content (presence of CO_3 groups confirmed by IR spectroscopy, see below) was calculated from the results of the crystal-structure refinement and on the basis of

P + C = 3 apfu, as the absence of CO_3 and OH in the channels was confirmed by IR spectroscopy. The results are reported in Table 2. The chemical formula obtained on the basis of 13 (O + F) pfu are $Ca_{4.90}\ Fe_{0.04}\ (PO_4)_{2.87}\ (CO_3)_{0.13}\ F_{1.23}$ (1.6 wt% CO_3) for FOW type-B CFAP, and $Ca_{4.97}\ Sr_{0.03}\ (PO_4)_{2.55}\ (CO_3)_{0.45}\ F_{1.42}$ (5.5 wt% CO_3) for FRA type-B CFAP. Both formulae show an excess of F > 1 pfu, which reasonably correlates with the CO_3 content.

Table 2

Electron microprobe analyses (mean of 10 analytical points, in wt%) of FOW and FRA samples, estimated standard deviation (esd) and relative formulae on the basis of 13 (O + F)

Sample Please split the words "Sample oxide" and wrap: Sample Oxide Note: "Sample" is referred to the two samples FOW and FRA. **oxide**	**FOW**			**FRA**		
	Average	**ESD** lowercase: esd	**Range**	**Average**	**ESD** lowercase: esd	**Ra**
FeO	0.59	0.13	0.36–0.80	0.01	0.01	0.0 0.0
CaO	54.99	0.20	54.67–55.30	56.29	0.15	55. 56.
SrO	0.04	0.02	0.03–0.09	0.65	0.11	0.3 0.7
P_2O_5	40.71	0.33	40.03–41.06	36.51	0.28	36. 36.
CO_2[a]	1.14			4.00		
F	4.69	0.10	4.55–4.86	5.43	0.20	5.2 5.7
Total	102.16	0.15	102.11–102.56	102.89	0.19	102 103
O=F	1.98	0.04	1.92–2.05	2.28	0.08	2.1 2.4

Calculated by stoichiometry

Total	100.18	0.15	100.09–100.55	100.61	0.18	100 101
P	2.868			2.549		
C^{4+}	0.130			0.450		
Σ T	2.998			2.999		
Fe^{2+}	0.041			0.001		
Ca	4.903			4.974		
Sr	0.002			0.031		
Σ cat	4.946			5.006		
F	1.235			1.415		
[a]Calculated by stoichiometry						

Two crystals of these carbonate-bearing fluorapatites (FOW size: 135 × 110 × 50 μm and FRA size: 100 × 80 × 60 μm) were selected on the basis of their optical features for single-crystal investigation. A preliminary characterization at room conditions was done using an Oxford Gemini R Ultra single-crystal X-ray diffractometer (CrisDi Centre, University of Torino), equipped with a CCD area detector, with graphite-monochromatized Mo*K*α radiation ($\lambda = 0.7107$ Å), and the tube operating at 50 kV and 40 mA. Diffraction data were collected in the 2θ range 0–82°. A total of 27 runs with 2806 frames (for FOW) and 2264 frames (for FRA) were collected, covering the whole accessible reciprocal space; 66,135 reflections of with 1209 unique were measured for FOW, and 66,143 of with 1210 unique for FRA. Omega-rotation frames (frame width 1°, exposure time 8 s, sample-to-detector distance 53 mm) were processed with the CrysAlisPro software (Agilent Technologies) and intensities were corrected for Lorentz and polarization effects. Data were corrected for empirical absorption. Scattering curves were chosen according to the calculated chemical formulae. All reflections with $I_o > 2\sigma(I)$ were considered as observed during weighted full-matrix least-squares refinement. Crystal-structure refinements were done in the space group $P6_3/m$, starting from the fractional coordinates of Comodi et al. (2001). Refinement of site scattering at the P sites showed a deficit. The maximum content of 15% CO_3 substitution at the P-sites did not produce evidence of site splitting in FOW CFAP (as it represents an electron density < 0.3 $e^-Å^{-3}$), whereas a maximum was clearly observed for FRA CFAP and was accordingly added to the model. The excess of fluoride was placed at the O3 oxygen site (the F3 site). Structural details were refined using the SHELX-97 package (Sheldrick 2008). Unit-cell parameters at room conditions are a =

9.3527(1), $c = 6.8752(1)$ Å, $V = 520.83(1)$ Å^3 for FOW CFAP, and $a = 9.3330(1)$, $c = 6.8984(1)$ Å, $V = 520.38(1)$ Å^3 for FRA CFAP, respectively. Anisotropic refinement with 45 parameters converged at $R = 0.018$ for 1170 reflections with $F_o \geq 4\sigma(F)$ and at $R = 0.020$ for all 1209 data for FOW CFAP. The refinement with 47 parameters converged at $R = 0.039$ for 1161 reflections with $F_o \geq 4\sigma(F)$ and at $R = 0.042$ for all 1210 data for FRA CFAP. Details of data collection and refinement for FOW and ~~Table 3.~~ FRA CFAP are listed in Table 3. Atom coordinates, displacement parameters and site occupancies are given in Table 4. Selected bond lengths are shown in Table 5 (CIF files deposited of Electronic supplementary material).

Table 3

Single-crystal data for FOW and FRA CFAP samples at ambient conditions (esd in parentheses)

	FOW	**FRA**
Space group	$P6_3/m$	$P6_3/m$
a (Å)	9.352-7 (1) please correct: 9.3527 (1)	9.3330 (1)
c (Å)	6.8752 (1)	6.8984 (1)
V (Å3)	520.83 (1)	520.38 (1)
Density (g/cm^3)	3.31	3.29
Refl. unique	1209	1210
Refl. F_0 please replace "zero" with the letter "o" replace F_0 with F_o $\geq 4\sigma(F)$	1170	1161
R (%) *all*	2.01	4.24
R (%) F_0 please replace "zero" with the letter "o" replace F_0 with F_o $\geq 4\sigma(F)$	1.84	3.96
Weight	0.05	0.09
Goodness of fit	1.15	2.53
$W = 1/[\sigma^2(F_0^2$ please replace "zero" with the letter "o" replace F_0^2 with F_o^2 $) + (a \cdot P)^2]$, where $P = (F_0^2$ please replace the "zero" with the letter "o" replace F_0^2 with F_o^2 $+ 2F_c^2)/3$		

Table 4

Atom coordinates, displacement parameters (Å^2) and site occupancies of FOW and FRA CF/

FOW						FRA	
Site	***x***	***Y*** lowercase: y	***Z*** lowercase: z	U_{eq} [a]	**s.o.f.** [b]	**Site**	***x***
Ca1	2/3	1/3	0.00113 (3)	0.01055 (6)	1.00 (1)	Ca1	2
Ca2	− 0.00730 (2)	0.24139 (2)	¼	0.00883 (5)	0.99 (1)	Ca2	− (
P	0.36903 (3)	0.39827 (3)	¼	0.00628 (7)	0.96 (1)	P	0 (
O1	0.48506 (10)	0.32724 (11)	¼	0.01188 (16)	1	O1	0 (
O O2 is correct please substitute O_2 with O2 2 O2 is correct please substitute O_2 with O2	0.46687 (11)	0.58793 (10)	1/4	0.01459 (17)	1	O O2 is correct please substitute O_2 with O2 2 O2 is correct please substitute O_2 with O2	0 (
O3	0.25709 (8)	0.34152 (9)	0.07053 (9)	0.01636 (14)	1.00 (2)	O3	0 (
						F3	0 (
F	0	0	1/4	0.0207 (3)	1	F	0
C	Not included into the refinement					C	0

All atoms except for C were refined with anisotropic-displacement parameters. Values w during the refinement. The combined occupancies of the C–P and O3–F3 pairs of atoms

[a] U_{eq} defined as one-third of the trace of the orthogonalized U_{ij} tensor

[b] s.o.f. = site occupancy factor; [c] U_{iso} (the isotropic displacement exponent) takes the forn

Table 5

Selected bond distances (Å) of FOW and FRA CFAP (esd in parentheses)

	FOW	**FRA**
Ca1–O1 (x3)	2.3914 (6)	2.3983 (11)
Ca1–O2 (x3)	2.4501 (6)	2.4561 (13)
Ca1–O3 (x3)	2.7983 (7)	2.7855 (15)
<Ca1–O>	2.547	2.547
Ca2–O1	2.6882 (9)	2.6816 (18)
Ca2–O2	2.3687 (9)	2.3709 (16)
Ca2–O3 (x2)	2.3461 (6)	2.3523 (12)
Ca2–O3′(x2)	2.4897 (7)	2.4896 (13)
<Ca2–O>	2.455	2.456
Ca2–F	2.2925 (2)	2.2819 (4)
Ca2–Ca2	3.9708 (3)	3.9523 (7)
P–O1	1.5298 (8)	1.5241 (16)
P– O O2 is correct please substitute O_2 with O2 2 O2 is correct please substitute O_2 with O2	1.5364 (9)	1.5250 (17)
P–O3 (x2)	1.5312 (6)	1.5352 (13)
<P–O>	1.532	1.530
C–O1	–	1.48 (2)
C– O O2 is correct please substitute O_2 with O2 2 O2 is correct please substitute O_2 with O2	–	1.45 (2)
C–O3	–	1.40 (3)
<C–O>		1.446

After characterization at room conditions, the two crystals of FOW and FRA CFAP were loaded concurrently into a ETH-type diamond-anvil cell (DAC, Miletich et al. 2000) for the high-pressure XRD investigations. A foil of T301 steel 250-µm thick was used as a gasket to hold the crystal, and it was pre-indented to 110 µm before drilling a hole by spark erosion (Ø 250 µm). A 16:3:1 mixture of methanol:ethanol:water was used as hydrostatic pressure-transmitting

medium (Angel et al. 2007; Klotz et al. 2009). The internal pressure and the uncertainty on *P* were calculated using a single crystal of quartz as an internal pressure calibrant (using 12 reflections) (Angel et al. 1997). The unit-cell parameters were please remove the dot and do not wrap .

~~Table 6~~ d ATTENTION: the sentence is attached to the previous one etermined at room temperature in the *P* range 0.0001–6.86 GPa (Table 6) from the setting angles of 19–21 reflections centered in eight positions (King and Finger 1979; Angel et al. 2000), using a Siemens P4 four-circle X-ray diffractometer (Department of Earth Sciences, University of Torino) with a point detector (graphite-monochromatized Mo*K*α radiation, θ-2θ scan mode, variable scanning speed 2.4–30°/min); the SINGLE Control Program software (Angel and Finger 2011) was used.

Table 6

Unit-cell parameters of FOW and FRA CFAP as a function of pressure (esd in parentheses)

P (GPa)	FOW			FRA		
	a (Å)	c (Å)	~~V~~ *V* (Å^3)	a (Å)	c (Å)	~~V~~ *V* (Å^3)
0.0001	9.3549 (8)	6.8739 (14)	520.97 (14)	9.330 (1)	6.8980 (14)	519.97(15)
0.02 (2)	9.3467 (8)	6.8704 (6)	519.79 (9)	9.3210 (11)	6.8976 (19)	518.98 (15)
0.25 (1)	9.3379 (8)	6.8665 (6)	518.52 (9)	9.310 (2)	6.895 (4)	517.5 (3)
0.72 (2)	9.3188 (8)	6.8590 (6)	515.84 (9)	9.2926 (14)	6.885 (2)	514.89 (19)
1.40 (2)	9.2940 (7)	6.8459 (6)	512.11 (9)	9.2699 (12)	6.869 (2)	511.19 (17)
1.62 (2)	9.2867 (8)	6.8429 (6)	511.09 (9)	9.2612 (11)	6.865 (2)	509.95 (16)
1.87 (2)	9.2788 (8)	6.8396 (6)	509.97 (9)	9.2527 (13)	6.861 (2)	508.69 (17)
2.18 (2)	9.2670 (8)	6.8336 (6)	508.23 (9)	9.2399 (12)	6.857 (2)	506.99 (16)
2.56 (2)	9.2530 (8)	6.8269 (6)	506.20 (10)	9.2282 (11)	6.8487 (19)	505.10 (15)
3.11 (3)	9.2336 (7)	6.8163 (5)	503.29 (8)	9.2088 (13)	6.836 (2)	502.03 (17)

Data collected during decompression

P (GPa)	FOW			FRA		
	a (Å)	c (Å)	~~V~~ V (Å)	a (Å)	c (Å)	~~V~~ V (Å)
3.31 (2)	9.2277 (7)	6.8132 (5)	502.42 (8)	9.2019 (12)	6.835 (2)	501.19 (16)
3.63 (2)	9.2183 (6)	6.8089 (5)	501.08 (7)	9.1925 (11)	6.8278 (19)	499.66 (15)
4.05 (2)	9.2051 (8)	6.8022 (6)	499.16 (9)	9.1778 (11)	6.818 (2)	497.38 (16)
4.41 (2)	9.1946 (7)	6.7959 (6)	497.55 (9)	9.1667 (11)	6.812 (2)	495.75 (15)
4.94 (3)	9.175 (4)	6.791 (4)	495.1 (5)	9.1527 (11)	6.805 (2)	493.71 (15)
5.25 (4)	9.1704 (10)	6.7843 (8)	494.10 (12)	9.1435 (11)	6.8015 (19)	492.44 (15)
5.64 (3)	9.1570 (10)	6.7771 (7)	492.14 (11)	9.1314 (11)	6.7953 (19)	490.70 (15)
5.91 (6)	9.1487 (7)	6.7727 (5)	490.91 (8)	9.1225 (10)	6.7885 (17)	489.26 (13)
6.36 (4)	9.1373 (8)	6.7660 (6)	489.22 (10)	9.1110 (10)	6.7824 (17)	487.58 (13)
6.55 (3)	9.1319 (7)	6.7640 (5)	488.49 (8)	9.1051 (13)	6.780 (2)	486.80 (17)
6.86 (4)	9.1220 (9)	6.7574 (7)	486.96 (10)	9.0954 (11)	6.7724 (19)	485.20 (15)
6.78 (4) [a]	9.1249 (8)	6.7589 (6)	487.37 (9)	9.0966 (12)	6.773 (2)	485.36 (15)
6.69 (5) [a]	9.1269 (8)	6.7596 (6)	487.64 (9)	9.1001 (10)	6.7764 (18)	485.98 (14)
6.52 (4)[a]	9.1324 (9)	6.7628 (7)	488.46 (10)	9.1048 (11)	6.779 (2)	486.64 (15)
5.83 (3)[a]	9.1500 (8)	6.7721 (6)	491.01 (9)	9.1247 (13)	6.789 (2)	489.52 (17)
5.38 (3)[a]	9.1635 (8)	6.7792 (6)	492.98 (10)	9.1365 (12)	6.797 (2)	491.35 (16)
3.31 (3)[a]	9.2247 (15)	6.8132 (12)	502.10 (18)	9.2020 (12)	6.832 (2)	501.01 (17)

[a]Data collected during decompression

Results and discussion

FTIR spectroscopy

The incorporation of carbonate in fluorapatite was investigated by Fourier transform infrared (FTIR) spectroscopy. Figure 1 shows the FTIR spectra (2000–700 cm^{-1}) for FOW (Fig. 1a) and FRA (Fig. 1b) fluorapatite samples. The spectra display the absorption bands characteristic of carbonate-bearing apatites (Elliott 2002). The prominent absorption band at around 1070 cm^{-1} and the weak peak at 965 cm^{-1} are due to stretching vibrations of the PO_4 groups. Both spectra of the CFAP samples exhibit the typical absorption bands of CO_3 groups in the spectral region 1400–1600 cm^{-1}. The asymmetric-stretching bands of CO_3 (ν_3) are observed at 1455 and 1430 cm^{-1}, and are characteristic of a type-B substitution, whereas the out-of-plane bending mode of CO_3 (ν_2) is observed at ~ 865 cm^{-1}, in agreement with those reported in the literature (Elliott 1994; Wilson et al. 2004; Fleet 2009; Yi et al. 2013). The carbonate-band intensities (absorbance) in the FRA spectrum (Fig. 1b) are higher than those in the FOW spectrum (Fig. 1a), indicating a larger amount of carbonate in the FRA sample, in accord with the carbonate contents determined by electron microprobe. There is no evidence of $(CO_3)^{2-}$ ions substituting for OH^- ions (type-A substitution), as the characteristic absorption at ~1545 cm^{-1} was not observed. In addition, no sharp peaks are observed in the OH-stretching region (3700–3100 cm^{-1}, not shown in Fig. 1) which indicates the absence of OH^- ions in the structure of the apatite samples examined.

Fig. 1

The Fourier-transform infrared (FTIR) spectra for **a** FOW and **b** FRA carbonate-bearing fluorapatite in the region 2000–700 cm^{-1}

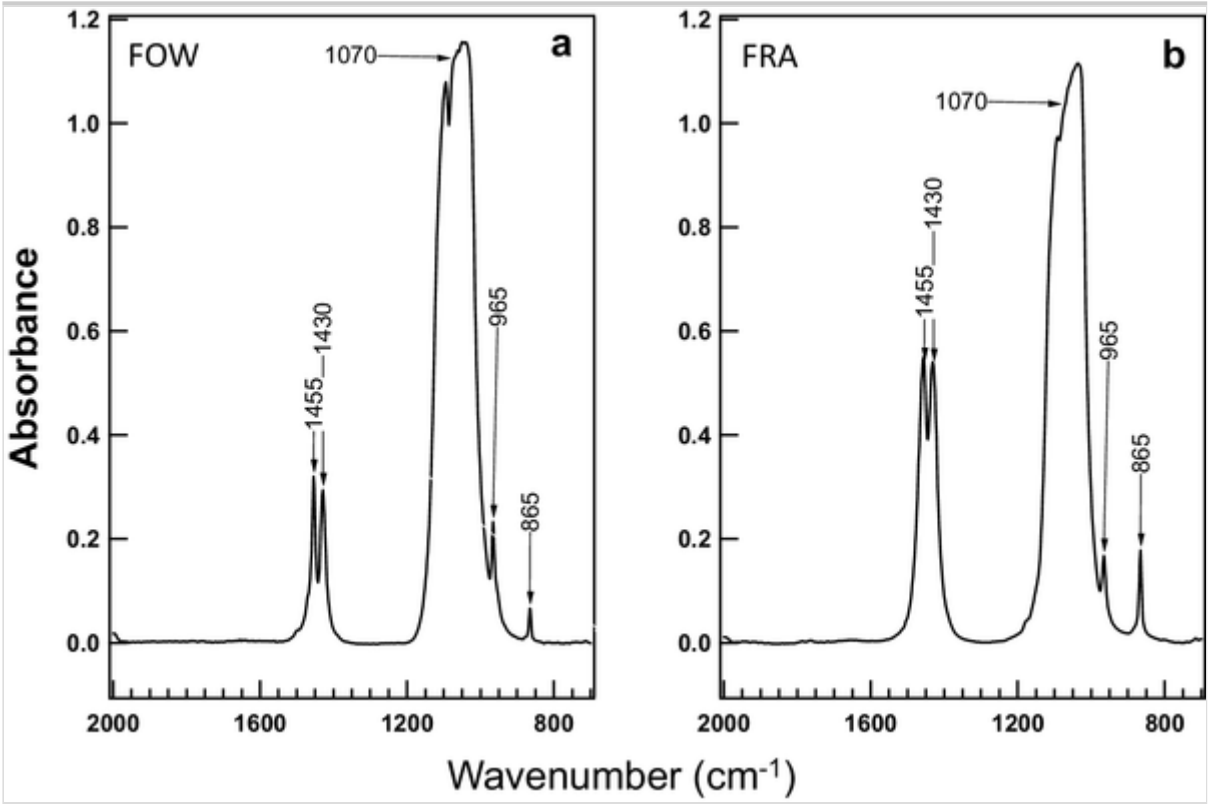

Structure refinement at room temperature

The chemical formulae of CFAP samples, obtained from electron microprobe analysis (Table 2) and FTIR spectra, indicate the presence of carbonate in both samples and show an excess of F. In their analysis of fluor-chlorapatite, Mackie and Young (1974) noted (F + Cl) > 2 halogen atoms per formula unit (apfu) for their two samples, both by chemical analysis (2.06, 2.25 halogen apfu for two samples) and by X-ray site refinement (2.09, 2.19 apfu). They proposed the presence of an additional Cl site at (0,0,0) that they could not asses from their results. The presence of this site was unassailable in the accurate work of Hughes et al. (2014) who found an 8% occupancy of Cl at (0,0,0). Yet their microprobe analyses, with their coincidence with the stoichiometry of the reactants, demonstrate that there are no excess halogens in the F–Cl anion column of their samples. Our refinement shows no residual electron density along (0,0,*z*). Therefore, we believe that F excess in our samples is related to type-B CO_3 in our samples.

The estimated amount of carbonate is 1.6 wt% for FOW CFAP and 5.5 wt% for FRA CFAP. The higher content of carbonate in FRA with respect to FOW is consistent with the observed *a* unit-cell parameter reduction from 9.3527(1) to 9.3330(1) Å and the significant increase of the *c* parameter from 6.8752(1) to 6.8984(1) Å (Table 3). The results of the structure refinement at room temperature (Table 4) show that, within FRA CFAP, the B carbonate ion is located close to the substituted phosphate group and the C atom~~s~~ occupies a

position (occupancy = 0.11) similar to the one observed by Wilson et al. (2004) in a sodium carbonate-bearing apatite and by Yi et al. (2013) in CFAP. In FOW CFAP, it was not possible to determine the position of the C atoms because of the low carbonate content.

As it is well known, within the type-B apatite the effect of the replacement of PO_4 ions by CO_3 ions on the structure is a reduction of the PO_4 tetrahedron volume together with a reduction of the P occupancy. Several studies (Elliott 1994; Wilson et al. 1999, 2004; Elliott et al. 2002) have noted that the occupancy of the phosphorus position gives the most reliable estimate of the extent of substitution by type-B carbonate. The occupancies of P in FOW and FRA CFAP (Table 4) become significantly less than unity, and these data are consistent with a substitution of the $(PO_4)^{3-}$ phosphate group by the $(CO_3)^{2-}$ carbonate ion. Within the FOW sample, the observed P occupancy is 0.96 (Table 4), equivalent to 2.88 P apfu, whereas, for the FRA sample, the observed P occupancy is 0.89, equivalent to 2.67 P apfu, i.e. substantially less than 3. The amounts of C atoms calculated directly from the P occupancies (C occ. = 0.04 and 0.11) are 0.12 and 0.33 apfu, respectively, in agreement with the chemical analyses (0.13 and 0.45). For the FRA sample, the occupancy of the O3 site (Table 4) becomes less than unity (0.96) whereas some F (occ. = 0.04) is present within the same site, which corresponds to 0.22 F apfu, lower than the amount found by electron probe analysis. With regard to the P-O distances, Table 5 shows that the replacement of P^{5+} ion by C^{4+} ion causes a deformation of the PO_4 tetrahedron, with changes in the P-O bond lengths as the CO_3 content increases. As expected, the P-O1 and P-O2 distances became shorter whereas the P-O3 distances increase slightly. This configuration is in agreement with the findings of Yi et al. (2013), who concluded from FTIR, ^{19}F DQ-SQ MAS NRM, and $^{13}C\{^{19}F\}$ frequency-selective REDOR experiments, that the planar carbonate oxyanion replacing the tetrahedral phosphate one, lies in the sloping face of the tetrahedron opposite to the fluoride ion occupying the remaining vertex. Yi et al. (2013) also propose a “francolite-type” diagnostic narrow IR absorption band at 864 cm^{-1} that is indeed present in our FTIR spectrum and its absorbance is proportional to the amount of this "francolite-type" defect (i.e. O by F substitution at the O3 site).

Elastic behavior and equation of state

The FOW and FRA unit-cell parameters determined up to $P = 6.86$ GPa are reported in Table 6 and the variation of *a* and c parameters and volume with pressure are shown in Figs. 2 and 3, respectively. No discontinuities that could be related to any possible phase transition are present up to 6.86 GPa. In the *P* range investigated, both *a* and *c* parameters decrease with increasing pressure

(Fig. 2). The linear compressibility coefficients are $\beta_a = 3.63 \times 10^{-3}$ GPa^{-1} and $\beta_c = 2.47 \times 10^{-3}$ GPa^{-1} for FOW, and $\beta_a = 3.67 \times 10^{-3}$ GPa^{-1} and $\beta_c = 2.65 \times 10^{-3}$ GPa^{-1} for FRA CFAP, giving an axial anisotropy of β_a:β_c = 1.47:1 and 1.38:1, respectively. As previously seen in Table 3, the higher content of carbonate in FRA CFAP causes the reduction of the *a* parameter and an increase of the *c* one with respect to FOW. The average compressibility of the cell volume is $\beta_V = 9.5 \times 10^{-3}$ GPa^{-1} for FOW and $\beta_V = 9.7 \times 10^{-3}$ GPa^{-1} for FRA.

Fig. 2

Variation of the *a* and *c* unit-cell parameters with pressure in FOW (filled circles) and FRA (open circles) CFAP. Lines are the EoS fit to the linear data (solid line: FOW; dashed line: FRA). Experimental uncertainties (bars) for almost all points are smaller than symbols

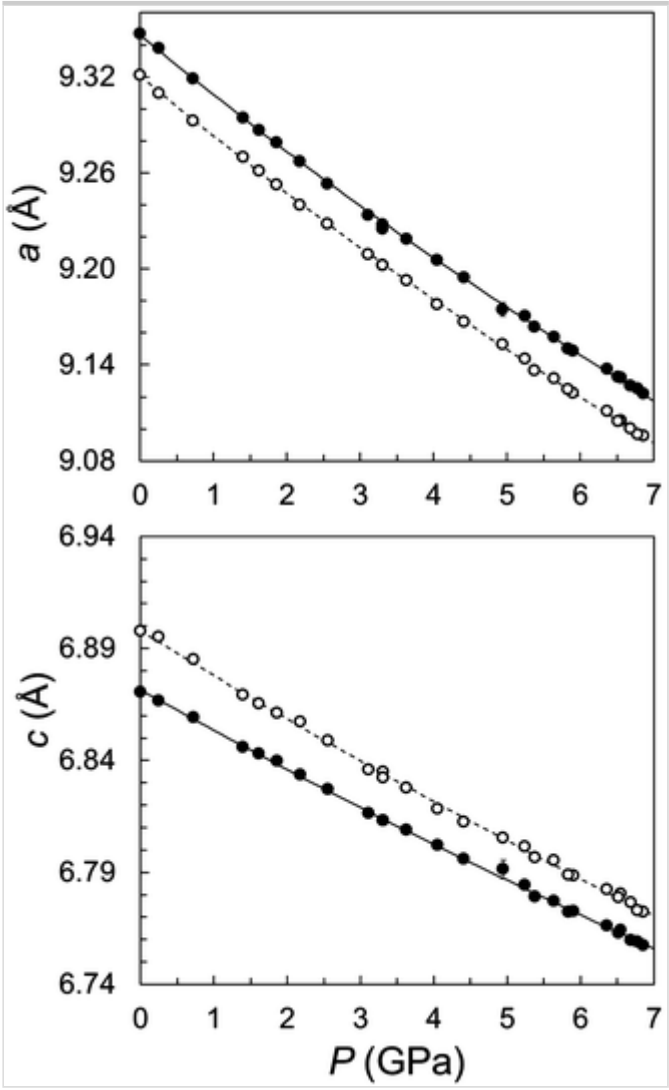

Fig. 3

Variation in unit-cell volume as a function of pressure for FOW and FRA CFAP. The lines show the second-order Birch–Murnaghan ~~e~~Equation of ~~s~~State (BM2-EoS) in the *P* range 0.0001–6.86 GPa. Symbols as in Fig. 2. Experimental uncertainties are smaller than symbols

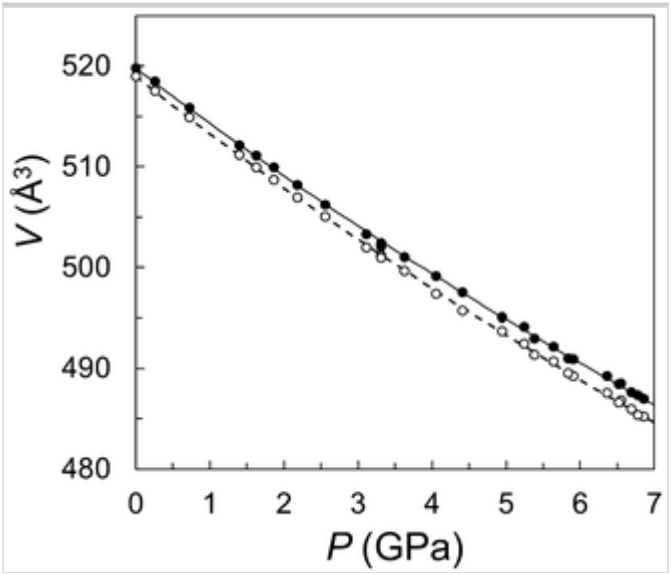

The *P*-*V* data (Fig. 3) were fitted by a third-order Birch–Murnaghan Equation of State (BM3-EoS) using 26 pressure points. The resulting EoS coefficients, calculated using the EosFit7 suite software (Angel et al. 2014; Gonzalez-Platas et al. 2016), are $V_0 = 519.93(8)$ Å^3, $K_{T0} = 89.9(1.1)$ GPa, $K' = 4.7(3)$ for FOW and $V_0 = 519.08(13)$ Å^3, $K_{T0} = 87.2(1.5)$ GPa, $K' = 4.6(4)$ for FRA CFAP. The isothermal bulk modulus of FRA is lower than that of FOW, indicating that carbonate content influences the compressibility of CFAP.

The confidence ellipses in K_{T0} and K' for the BM3 EoS fit are reported in Fig. 4 and confirm that the compressibility of FRA CFAP (dashed line) is higher than that of FOW.

Fig. 4

Confidence ellipses in K_{T0} and K' for the fit of the third-order Birch–Murnaghan EoS to the fluorapatite *P*-*V* data at 95.4% level (2σ) (solid line: FOW; dashed line: FRA)

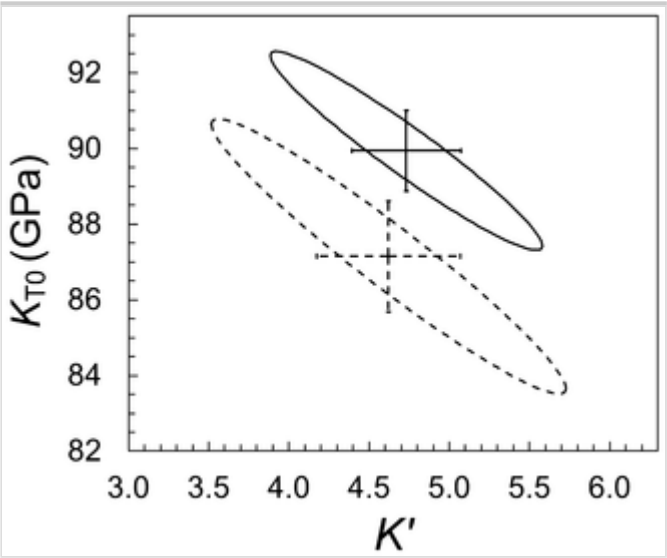

When our *P*-*V* data are reformulated as a normalized pressure —- finite strain plot (F_E - f_E plot, Angel 2000) (Fig. 5), the values lie on a horizontal line of constant F_E ($K' = 4$), indicating that the data are adequately described by a BM2-EoS. Therefore, the data can be fitted by a second-order truncation of the Birch–Murnaghan Equation of State. Fitting the *P*-*V* data to a BM2-EoS gives the resulting coefficients of $V_0 = 519.81(7)$ Å^3, $K_{T0} = 92.1(3)$ GPa for FOW and of $V_0 = 518.95(9)$ Å^3, $K_{T0} = 89.1(4)$ GPa for FRA samples (Table 1). BM2-EoS gives higher bulk moduli for both samples with respect to BM3-EoS, and confirms that type-B carbonate substitution reduces the isothermal bulk modulus of FAP.

Fig. 5

Normalized pressure F_E versus Eulerian finite strain f_E in FOW and FRA CFAP ($F_E = P/3 \times f_E \times (1 + 2 f_E)^{5/2}$ and $f_E = [(Vo/V)^{2/3} - 1]/2$, Angel 2000). The horizontal lines of constant F_E indicate that the *P*-*V* data could be fitted by a second-order truncation of the BM-EoS for both apatites. Symbols as in Fig. 2. Bars indicate experimental uncertainties

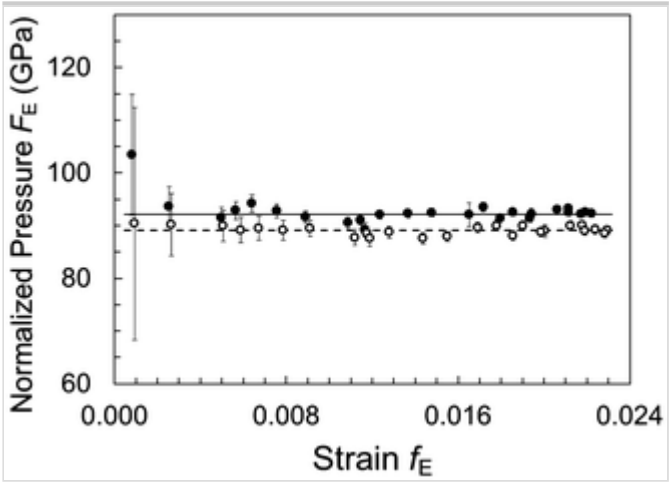

Figure 6 shows the variation of both *a* and *c* unit-cell parameters for FOW and FRA CFAP as function of pressure, normalized to their room-pressure values. Compressibilities along unit-cell axes were determined by fitting a BM2-EoS to *a* and *c* parameters in the range 0.0001–6.86 GPa. The coefficients obtained are $a_0 = 9.3461(5)$ Å, 1/3 $M_i = 81.2(3)$ GPa; $c_0 = 6.8716(4)$ Å, 1/3 $M_i = 124.2(7)$ GPa for FOW, and $a_0 = 9.3204(7)$ Å, 1/3 $M_i = 80.7(4)$ GPa; $c_0 = 6.8981(10)$ Å, 1/3 $M_i = 111.9(1.4)$ GPa for FRA, respectively (with i = *a, c* and the linear moduli $M_i = \beta_i^{-1}$, Angel et al. 2014). The linear moduli indicate axial-compression anisotropy with $\beta_a > \beta_c$ and confirm that the *a*-axis direction is more compressible than *c*-axis direction for both samples. As the ~~elastic anisotropy (~~M_c:M_a~~)~~ ratios for ~~of~~ FOW and FRA are ~~a little different (~~1.53 and 1.39, respectively~~)~~, the two samples of CFAP show quite different elastic anisotropy~~, as seen in~~ (Fig. 6). The effect of incorporation of type-B carbonate is, therefore, stronger on the compressibility along the *c*-axis.

Fig. 6

Variation of *a* and *c* unit-cell parameters of FOW and FRA CFAP as a function of pressure, normalized to their room-pressure values. Symbols as in Fig. 2. Lines correspond to linear fits in the *P* range 0.0001–6.86 GPa with linear moduli M_i = 244(1) and 372(2) GPa for FOW and 242(1) and 336(4) GPa for FRA (with i = *a, c* and $M_i = \beta_i^{-1}$, Angel et al. 2014). Experimental uncertainties (bars) for almost all points are smaller than symbols

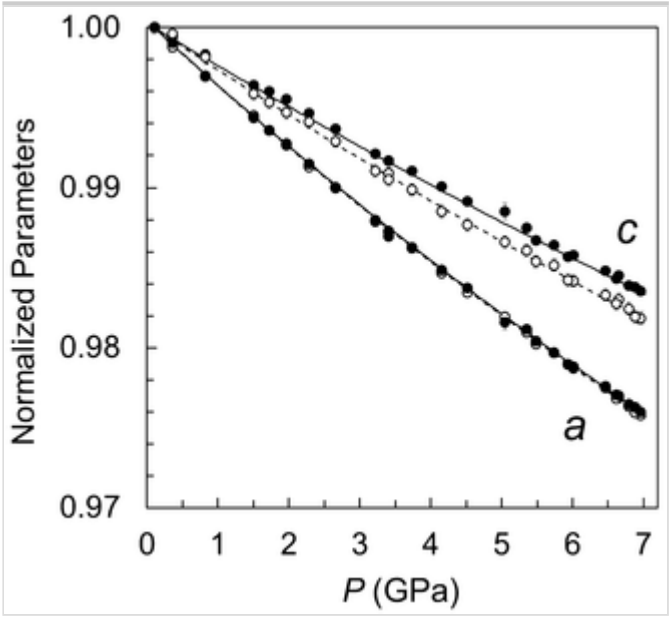

Figure 7 compares the bulk modulus, as a function of carbonate content within both FOW and FRA CFAP, with the values obtained by the compressibility experiments on apatite. In Fig. 7a the bulk moduli for FOW and FRA type-B carbonate-bearing FAP samples, along with those obtained on synthetic carbonate-free fluorapatites (Brunet et al. 1999; Comodi et al. 2001) are showed. Considering the values of K_{T0} obtained on FAP (Table 1), our results show that a 5.5 wt% carbonate content has a considerable effect on the elastic properties and significantly reduces the bulk modulus of FAP by about 9%. The very low values obtained by Matsukage et al. (2004) and Schouwink et al. (2010) in their FPA (Table 1) disagree with our results, probably because of the 5–6 mol% of chlorapatite content of their samples. Our results on the compressibility of CFAP are in good agreement with those obtained by Liu et al. (2011) on synthetic type A-B CHAP. In fact, the results of their high-pressure experimental investigation up to 10 GPa (LM006 and LM005 samples in Fig. 7b) show that the isothermal bulk modulus in hydroxylapatite is significantly reduced (about 15%) by a carbonate content up to 11 wt%.

Fig. 7

Bulk modulus (K_{T0}) as a function of carbonate content (wt% CO_3) for **a** fluorapatite and **b** hydroxylapatite. **a** Square: carbonate-free fluorapatite (Brunet et al. 1999); triangle: carbonate-free fluorapatite (Comodi et al. 2001); filled circle: FOW and open circle: FRA carbonate-bearing fluorapatites (this work). **b** Diamond: carbonate-free hydroxylapatite (Brunet et al. 1999); asterisks: carbonate-rich hydroxylapatite (LM006 and LM005 samples, Liu et al. 2011)

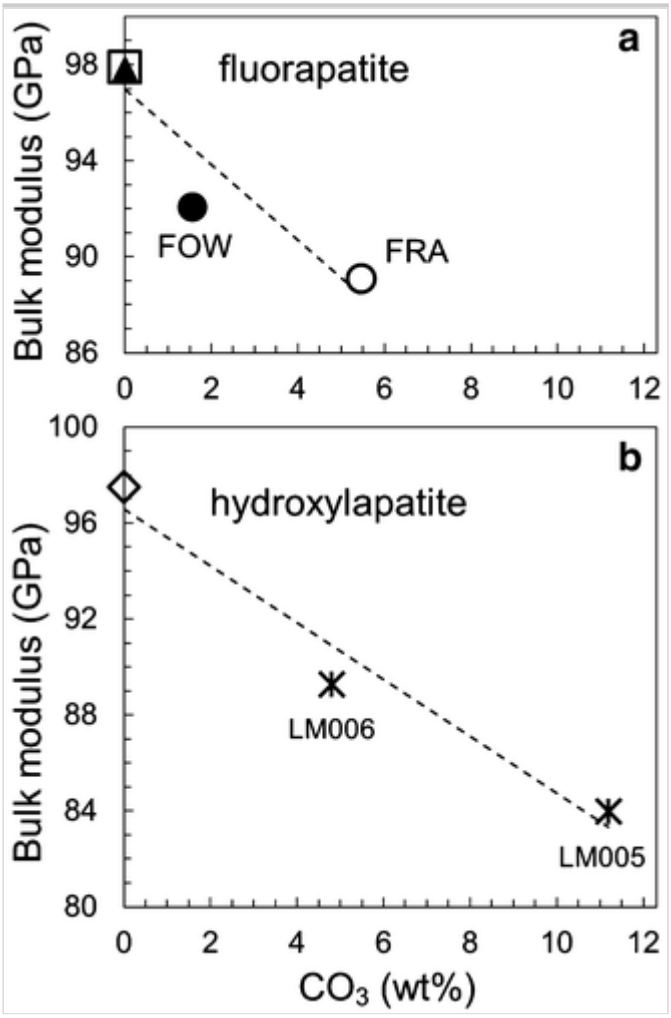

Conclusion

The substitution of the carbonate ion for either the monovalent channel anion (type-A substitution) or for the oxyanion ZO_4^{3-} (type-B substitution) is of particular biological and mineralogical interest. The HAP is the mineral species most similar to the inorganic component of bones; the carbonate is present within bone in a range of concentrations from ~5 to 8 wt%, and ~2 to 4 wt% in enamel, substituting primarily for phosphate (Pasteris 2016). Apatite is the necessary hard phase in natural bone and, therefore, its elastic properties are particularly important for the design of bioapatite substitutes (prosthesis). Powdered FAP is used in dental applications. In fact, fluorine hosted by CHAP is the important anticaries component of the dental enamel; there is only ~ 100 ppm F in the interior of dental enamel (Elliott 2002) but up to 1 wt% in the outermost micrometer-scale layer (Brudevold et al. 1956). Moreover, FAP is a potential host for the containment of high-level nuclear waste, as indicated by its occurrence in the natural reactor at Oklo, Gabon (Bros et al. 1996).

Our study confirms the anisotropic elastic behavior of apatite, even in the presence of less common components as the CO_3. This has to be considered

when elasticity of apatite is used for pressure determination like apatite-in-garnet barometer used by Ashley et al. (2017) because as discussed by Angel et al. (2015) the anisotropic behavior of the inclusion can modify the elastic response of the inclusion. In fact, the anisotropy could be treated as a deviatoric effect relative to the isotropic case (Angel et al. 2015).

Whereas there has been discussion on the carbonate substitution in fluorapatite, CFAP with only B carbonate has not been studied so far by single-crystal X-ray structure refinement (Fleet and Liu 2008a). Additionally, prior to the present study, there were no data available on the elastic properties of CFAP. The results of this study show that the replacement of P by $(CO_3)^{2-}$ (type-B substitution) involves a softening of the bulk modulus, as previously observed in CHAP (Liu et al. 2011). Whereas data on CHAP cannot discern between the role of type-A and type-B substitutions (as the samples studied by Liu et al. 2011 contained both types of substitution), the results of our study clearly reinforce the prominent role of type-B substitution in the softening.

Acknowledgements

Ravinder Sidhu is thanked for support with EMP analysis (Winnipeg). Ross J. Angel is thanked for assessment with the installation of SINGLE software at Department of Earth Sciences, University of Torino, and for making available several very useful software applications in his Web site. We are grateful to Matteo Alvaro for helpful suggestions. We thank John M. Hughes and an anonymous referee for critical reading and useful suggestions that greatly improved the manuscript. The CrisDi and Scansetti Interdepartmental Centres of University of Torino are thanked. Financial support has been provided by “Ministero dell’Istruzione, dell’Università e della Ricerca” (MIUR), MIUR-Project PRIN 2010–2011, 2010EARRRZ_007 “Crystal-chemical and structural investigations on the bulk and surfaces of carbonated apatites with amorphous and nano-crystal transitions”. FCH acknowledges support by a Canada Research Chair in Crystallography and Mineralogy and by a Discovery Grant from the Natural Sciences and Engineering Research Council of Canada, and by Innovation Grants from the Canada Foundation for Innovation.

Electronic supplementary material

Below is the link to the electronic supplementary material.

Supplementary material 1 (CIF 56 KB)

References

Allan DR, Angel RJ, Miletich R, Reichmann H, Brunet F (1996) High-pressure powder-diffraction studies of apatite $(Ca_5PO_4)_3(OH, F, Cl)$. Exp N° HC439, ESRF Report

Angel RJ (2000) Equations of state. In: Hazen RM, Downs RT (eds) High-temperature and high-pressure crystal chemistry, vol 41, pp 35–59. Reviews in Mineralogy and Geochemistry, Mineralogical Society of America and Geochemical Society, Chantilly, Virginia. https://doi.org/10.2138/rmg.2000.41.2

Angel RJ, Finger LW (2011) SINGLE: a program to control single-crystal diffractometers. J Appl Crystallogr 44:247–251. https://doi.org/10.1107/S0021889810042305

Angel RJ, Allan DR, Miletich R, Finger LW (1997) The use of quartz as an internal pressure standard in high-pressure crystallography. J Appl Crystallogr 30:461–466. https://doi.org/10.1107/S0021889897000861

Angel RJ, Downs RT, Finger LW (2000) High-temperature - high-pressure diffractometry. In: Hazen RM, Downs RT (eds) High-temperature and high-pressure crystal chemistry, vol 41, pp 559–597. Reviews in Mineralogy and Geochemistry, Mineralogical Society of America and Geochemical Society, Chantilly, Virginia. https://doi.org/10.2138/rmg.2000.41.16

Angel RJ, Bujak M, Zhao J, Gatta GD, Jacobsen SD (2007) Effective hydrostatic limits of pressure media for high-pressure crystallographic studies. J Appl Crystallogr 40:26–32. https://doi.org/10.1107/S0021889806045523

Angel RJ, Gonzalez-Platas J, Alvaro M (2014) EosFit7c and a Fortran module (library) for equation of state calculations. Z Kristallogr 229:405–419. https://doi.org/10.1515/zkri-2013-1711

Angel RJ, Nimis P, Mazzucchelli ML, Alvaro M, Nestola F (2015) How large are departures from lithostatic pressure? Constraints from host–inclusion elasticity. J Metamorph Geol 33:801–813. https://doi.org/10.1111/jmg.12138

Ashley KT, Barkoff DW, Steele-MacInnis M (2017) Barometric constraints based on apatite inclusions in garnet. Am Mineral 102:743–749. https://doi.org/10.2138/am-2017-5898

Bros R, Carpena J, Sere V, Beltritti A (1996) Occurrence of Pu and fissiogenic REE in hydrothermal apatites from the fossil nuclear reactor 16 at Oklo (Gabon). Radiochim Acta 74:277–282

Brudevold F, Gardner DE, Smith FA (1956) The distribution of fluoride in human enamel. J Dent Res 35:420–429. https://doi.org/10.1177/00220345560350031301

Brunet F, Allan DR, Redfern SAT, Angel RJ, Miletich R, Reichmann HJ, Sergent J, Hanfland M (1999) Compressibility and thermal expansivity of synthetic apatites, $Ca_5(PO_4)_3X$ with X = OH, F and Cl. Eur J Mineral 11:1023–1035. https://doi.org/10.1127/ejm/11/6/1023

Comodi P, Liu Y (2000) CO_3 substitution in apatite: further insight from new crystal-chemical data of Kasekere (Uganda) apatite. Eur J Mineral 12:965–974. https://doi.org/10.1127/ejm/12/5/0965

Comodi P, Liu Y, Zanazzi PF, Montagnoli M (2001) Structural and vibrational behaviour of fluorapatite with pressure. Part I: in situ single-crystal X-ray diffraction investigation. Phys Chem Miner 28:219–224. https://doi.org/10.1007/s002690100154

Elliott JC (1994) Structure and chemistry of the apatites and other calcium orthophosphates. Elsevier, Amsterdam

Elliott JC (2002) Calcium phosphate biominerals. In: Kohn MJ, Rakovan J, Hughes JM (eds) Phosphates: geochemical, geobiological and materials importance, vol 48, pp 427–454. Reviews in Mineralogy and Geochemistry, Mineralogical Society of America, Chantilly, Virginia. ISBN 0-939950-60-X

Elliott JC, Wilson RM, Dowker SEP (2002) Apatite structures. Advances in X-ray analysis. Copyright (c)JCPDS ICDD, vol 45, pp 172–181

Fleet ME (2009) Infrared spectra of carbonate apatites: ν_2-region bands. Biomaterials 30:1473–1481. https://doi.org/10.1016/j.biomaterials.2008.12.007

Fleet ME, Liu X (2004) Location of type B carbonate ion in type A-B carbonate apatite synthesized at high pressure. J Solid State Chem 177:3174–3182. https://doi.org/10.1016/j.jssc.2004.04.002

Fleet ME, Liu X (2007) Coupled substitution of type A and B carbonate in sodium-bearing apatite. Biomaterials 28:916–926. https://doi.org/10.1016/j.biomaterials.2006.11.003

Fleet ME, Liu X (2008a) Accommodation of the carbonate ion in fluorapatite synthesized at high pressure. Am Mineral 93:1460–1469. https://doi.org/10.2138/am.2008.2786

Fleet ME, Liu X (2008b) Type A-B carbonate chlorapatite synthesized at high pressure. J Solid State Chem 181:2494–2500. https://doi.org/10.1016/j.jssc.2008.06.016

Fleet ME, Liu X, King PL (2004) Accommodation of the carbonate ion in apatite: an FTIR and X-ray structure study of crystals synthesized at 2–4 GPa. Am Mineral 89:1422–1432

Gonzalez-Platas J, Alvaro M, Nestola F, Angel RJ (2016) EosFit7-GUI: a new graphical user interface for equation of state calculations, analyses and teaching. J Appl Crystallogr 49:1377–1382. https://doi.org/10.1107/S1600576716008050

Henry TH (1850) On francolite, a supposed new mineral. Philos Mag 36:134–135

Hughes JM (2015) The many facets of apatite. Am Mineral 100:1033–1039. https://doi.org/10.2138/am-2015-5193

Hughes JM, Rakovan J (2002) The crystal structure of apatite, $Ca_5(PO_4)_3(F,OH,Cl)$. In: Kohn MJ, Rakovan J, Hughes JM (eds) Phosphates: geochemical, geobiological and materials importance, vol 48, pp 1–12. Reviews in Mineralogy and Geochemistry, Mineralogical Society of America, Chantilly, Virginia. ISBN 0-939950-60-X

Hughes JM, Rakovan JF (2015) Structurally robust, chemically diverse: apatite and apatite supergroup minerals. Elements 11:165–170. https://doi.org/10.2113/gselements.11.3.165

Hughes JM, Cameron M, Crowley KD (1989) Structural variations in natural F, OH and Cl apatites. Am Mineral 74:870–876

Hughes JM, Cameron M, Crowley KD (1990) Crystal structures of natural ternary apatites: solid solution in the $Ca_5(PO_4)_3X$ (X = F, OH, Cl) system. Am Mineral 75:295–304

Hughes JM, Nekvasil H, Ustunisik G, Lindsley DH, Coraor AE, Vaughn J, Phillips B, McCubbin FM, Woerner WR (2014) Solid solution in the fluorapatite-chlorapatite binary system: High-precision crystal structure refinements of synthetic F-Cl apatite. Am Mineral 99:369–376. https://doi.org/10.2138/am.2014.4644

Ivanova TI, Frank-Kamenetskaya OV, Kol'tsov AB, Ugolkov VL (2001) Crystal structure of calcium-deficient carbonated hydroxyapatite. Thermal decomposition. J Solid State Chem 160:340–349. https://doi.org/10.1006/jssc.2000.9238

King HE, Finger LW (1979) Diffracted beam crystal centering and its application to high-pressure crystallography. J Appl Crystallogr 12:374–378. https://doi.org/10.1107/S0021889879012723

Klotz S, Chervin JC, Munsch P, Marchand G Le (2009) Hydrostatic limits of 11 pressure transmitting media. J Phys D Appl Phys 42(7 pp):75413. https://doi.org/10.1088/0022-3727/42/7/075413

Knudsen AC, Gunter ME (2002) Sedimentary phosphorites - an example: Phosphoria Formation, Southern Idaho, USA. In: Kohn MJ, Rakovan J, Hughes JM (eds) Phosphates: geochemical, geobiological and materials importance, vol 48, pp 363–389. Reviews in Mineralogy and Geochemistry, Mineralogical Society of America, Chantilly, Virginia. ISBN 0-939950-60-X

LeGeros RZ (1965) Effect of carbonate on the lattice parameters of apatite. Nature 206:403–404

LeGeros RZ (1991) Calcium phosphates in oral biology and medicine. Karger, New York. https://doi.org/10.1159/isbn.978-3-318-04021-0

Leventouri TH, Chakoumakos BC, Moghaddam HY, Perdikatsis V (2000) Powder neutron diffraction studies of a carbonate fluorapatite. J Mater Res

15:511–517

Liu X, Shieh SR, Fleet ME, Zhang L, He Q (2011) Equation of state of carbonated hydroxylapatite at ambient temperature up to 10 GPa: Significance of carbonate. Am Mineral 96:74–80. https://doi.org/10.2138/am.2011.3535

Mackie PE, Young RA (1974) Fluorine-chlorine interaction in fluor-chlorapatite. J Solid State Chem 11:319–329. https://doi.org/10.1016/S0022-4596(74)80037-X

Matsukage KN, Ono S, Kawamoto T, Kikegawa T (2004) The compressibility of a natural apatite. Phys Chem Miner 31:580–584. https://doi.org/10.1007/s00269-004-0415-x

McClellan GH (1980) Mineralogy of carbonate fluorapatites. J Geol Soc London 137:675–681

McClellan GH, Lehr JR (1969) Crystal chemical investigation of natural apatites. Am Mineral 54:1374–1391

McClellan GH, Van Kauwenbergh SJ (1990) Mineralogy of sedimentary apatites. In: Notholt AJG, Jarvis I (eds) Phosphorite research and development-Geol Soc London Spec Pub vol 52, pp 23–31. https://doi.org/10.1144/GSL.SP.1990.052.01.03

McConnell D (1938) A structural investigation of the isomorphism of the apatite group. Am Mineral 23:1–19

McCubbin FM, Mason HE, Park H, Phillips BL, Parise JB, Nekvasil H, Lindsley DH (2008) Synthesis and characterization of low-OH^- fluor-chlorapatite: a single-crystal XRD and NMR spectroscopic study. Am Mineral 93:210–216. https://doi.org/10.2138/am.2008.2557

Miletich R, Allan DR, Kuhs WF (2000) High-pressure single-crystal techniques. In: Hazen RM, Downs RT (eds) High-temperature and high-pressure crystal chemistry, vol 41, pp 445–519. Reviews in Mineralogy and Geochemistry, Mineralogical Society of America and Geochemical Society, Chantilly, Virginia. https://doi.org/10.2138/rmg.2000.41.14

Nathan Y (1996) Mechanism of CO_3^{2-} substitution in carbonate-fluorapatite: evidence from FTIR spectroscopy, ^{13}C NMR, and quantum mechanical calculations - discussion. Am Mineral 81:513–514

Pan Y, Fleet ME (2002) Compositions of the apatite-group minerals: Substitution mechanisms and controlling factors. In: Kohn MJ, Rakovan J, Hughes JM (eds) Phosphates: geochemical, geobiological and materials importance, vol 48, pp 13–49. Reviews in Mineralogy and Geochemistry, Mineralogical Society of America, Chantilly, Virginia. ISBN 0-939950-60-X

Pasero M, Kampf AR, Ferraris C, Pekov IV, Rakovan J, White TJ (2010) Nomenclature of the apatite supergroup minerals. Eur J Mineral 22:163–179. https://doi.org/10.1127/0935-1221/2010/0022-2022

Pasteris JD (2016) A mineralogical view of apatitic biomaterials. Am Mineral 101:2594–2610. https://doi.org/10.2138/am-2016-5732

Perdikatsis B (1991) X-ray powder diffraction study of francolite by the Rietveld method. Mater Sci Forum, vols 79–82, 809–814

Pouchou JL, Pichoir F (1985) 'PAP' φ(ρZ) procedure for improved quantitative microanalysis. In: Armstrong JT (ed) Microbeam analysis. San Francisco Press, San Francisco, pp 104–106

Rakovan JF, Pasteris JD (2015) A technological gem: materials, medical, and environmental mineralogy of apatite. Elements 11:195–200. https://doi.org/10.2113/gselements.11.3.195

Regnier P, Lasaga AC, Berner RA, Han OH, Zilm KW (1994) Mechanism of CO_3^{2-} substitution in carbonate-fluorapatite: evidence from FTIR spectroscopy, ^{13}C NMR, and quantum mechanical calculations. Am Mineral 79:809–818

Sandell EB, Hey MH, McConnell D (1939) The composition of francolite. Min Mag 25:395–401

Schouwink P, Miletich R, Ullrich A, Glasmacher UA, Trautmann C, Neumann R, Kohn BP (2010) Ion tracks in apatite at high pressures: the effect of crystallographic track orientation on the elastic properties of

fluorapatite under hydrostatic compression. Phys Chem Miner 37:371–387. https://doi.org/10.1007/s00269-009-0340-0

Sheldrick GM (2008) A short history of SHELX. Acta Cryst A 64:112–122. https://doi.org/10.1107/S0108767307043930

Wilson RM, Elliott JC, Dowker SEP (1999) Rietveld refinement of the crystallographic structure of human dental enamel apatites. Am Mineral 84:1406–1414

Wilson RM, Elliott JC, Dowker SEP, Smith RI (2004) Rietveld structure refinement of precipitated carbonate apatite using neutron diffraction data. Biomaterials 25:2205–2213. https://doi.org/10.1016/j.biomaterials.2003.08.057

Yi H, Balan E, Gervais C, Segalen L, Fayon F, Roche D, Person A, Morin G, Guillaumet M, Blanchard M, Lazzeri M, Babonneau F (2013) A carbonate-fluoride defect model for carbonate-rich fluorapatite. Am Mineral 98:1066–1069. https://doi.org/10.2138/am.2013.4445